Recombination between co-infecting herpesviruses occurs where replication compartments coalesce

Enosh Tomer[a], Efrat M. Cohen[a], Nir Drayman[b], Amichay Afriat[a], Matthew D. Weitzman[c,d], Assaf Zaritsky[e] and Oren Kobiler[a]*

[a]Department of Clinical Microbiology and Immunology, Sackler School of Medicine, Tel Aviv University, Tel Aviv, Israel

[b]Institute for Genomics and Systems Biology and Institute for Molecular Engineering, University of Chicago, Chicago, IL, USA

[c]Department of Pathology and Laboratory Medicine, Perelman School of Medicine, University of Pennsylvania, Philadelphia, PA, USA

[d]Division of Protective Immunity, Children's Hospital of Philadelphia, Philadelphia, PA, USA

[e] Department of Software and Information Systems Engineering, Ben-Gurion University of the Negev, Be'er Sheva, Israel.

Running title:

HSV-1 recombination at colaescing replication compartments

* Corresponding author: Oren Kobiler, okobiler@post.tau.ac.il

Abstract

Homologous recombination (HR) is considered a major driving force of evolution since it generates and expands genetic diversity. Evidence of HR between co-infecting herpesvirus DNA genomes can be found frequently, both *in vitro* and in clinical isolates. Each herpes simplex virus type 1 (HSV-1) replication compartment (RC) derives from a single incoming genome and maintains a specific territory within the nucleus. This raises intriguing questions about where and when co-infecting viral genomes interact. To study the spatiotemporal requirements for inter-genomic recombination, we developed an assay with dual-color fluorescence *in situ* hybridization which enables detection of HR between different pairs of co-infecting HSV-1 genomes. Our results revealed that when viral RCs enlarge towards each other, there is detectable overlap between territories of genomes from each virus. Infection with paired viruses that allow visualization of HR correlates with increased overlap of RCs. Further, inhibition of RC movement reduces the rate of HR events among co-infecting viruses. Taken together, these findings suggest that inter-genomic HR events take place during replication of HSV-1 DNA and are mainly confined to the periphery of RCs when they coalesce. Our observations have implications on understanding the recombination restrictions of other DNA viruses and cellular DNA.

41 **Introduction**

42 Recombination is considered to be a major driving force in evolution of most organisms,
43 since it accelerates adaptation (1,2). The architecture of eukaryotic nuclei is suggested
44 to regulate many DNA-mediated processes, including replication, gene expression
45 and recombination. DNA viruses that replicate inside the nucleus clearly change the
46 nuclear architecture, however they are subjected to similar spatial constraints as host
47 DNA. The rate of mutation accumulation is lower for DNA viruses than that of viruses
48 with RNA genomes (3,4). It has been hypothesised that high rates of recombination
49 can facilitate genetic adaptation to the changing environment (5). Indeed, homologous
50 recombination (HR) among co-infecting Herpes simplex virus type 1 (HSV-1) genomes
51 is very frequently observed in both *in vitro* genetic assays (6-12) and in sequence
52 analysis of clinical isolates (13-15). Herpesvirus infection therefore provide a system
53 to study spatial features that promote or constrain recombination in the eukaryotic
54 nucleus.

55 Like all other herpesviruses, HSV-1 viral gene expression, replication and capsid
56 assembly all occur in the host nucleus of infected cells. Viral genomes enter the
57 nucleus through the nuclear pore complex as naked DNA molecules (16), and these
58 rapidly recruit several host and viral proteins to the viral genomes (17-25). Expression
59 of the immediate early and early viral genes allows initiation of viral DNA replication
60 (26). HSV-1 DNA replication proceeds at distinct foci within the nucleus known as
61 replication compartments (RCs) (27,28). The formation of the viral RCs was suggested
62 to initiate from small pre-RCs (29,30). Live cell imaging of viral DNA binding proteins
63 suggested that the pre-RCs migrate toward nuclear speckles, sites of RNA processing,
64 and come into contact with other pre-RCs, where they seem to coalesce into large
65 mature RCs (31). On the other hand, direct visualization of the viral DNA suggested

66 that each RC usually emerges from a single incoming genome (32,33). Our previous
67 study with the swine alphaherpesvirus Pseudorabies virus (PRV) suggested that
68 although viral replication compartments are found in close proximity, they retain
69 distinct territories for each individual genome (33). Earlier experiments with HSV
70 replicons also supported this notion (32). A recent study showed that viral genomes
71 entering the nucleus are observed as condensed foci, and suggested that viral
72 expression and DNA replication allow decondensation of these genomes and
73 formation of RCs (34). Interestingly, some genomes remain highly condensed at the
74 edge of newly developing RCs (34,35). Here, we visualised co-infecting HSV-1
75 genomes and confirmed that alphaherpesviruses RCs initiate from single genomes.

76 Viral DNA recombination is facilitated by both viral and cellular proteins. Two viral
77 proteins have been suggested to work as a complex to facilitate viral recombination
78 and have been shown to catalyze strand exchange *in vitro*: the single strand binding
79 protein ICP8 and an exonuclease UL12 (36). Single strand annealing was found to be
80 a recombination mechanism upregulated during viral infection and thus is considered
81 as the mechanism by which the viral recombinase induces recombination (37). While
82 ICP8 is required for viral DNA replication, UL12 is not essential for DNA replication *per*
83 *se*, although it is required for formation of infectious viral genomes that can be
84 packaged into capsids (38). Recent observations suggest a complex relationship
85 between HSV and the host DNA repair machinery. Some components of the DNA
86 damage response (DDR) machinery are recruited to replicating viral DNA, where they
87 may function in ways that are beneficial for viral progeny (12,21,23,39-42). In contrast,
88 DDR pathways as a whole may be considered to be anti-viral and are suppressed in
89 HSV-infected cells (19,43-48). These findings suggest that the processes of viral
90 recombination and viral replication are intimately associated (46). While knowledge

91 regarding the molecular aspects of HR has been accumulating over the last few years,
92 little is known regarding spatiotemporal constraints on inter-genomic recombination.

93 The compartmentalization of co-infecting genomes at different RCs raises questions
94 about where and when recombination takes place during the course of infection. To
95 tackle these questions, we utilized a fluorescence *in situ* hybridization (FISH) based
96 assay to differentiate between *de-novo* synthesized variants of viral genomes. Our
97 results suggest that multiple inter-genomic recombination events occur at later stages
98 of infection following DNA replication, and that inter-genomic recombination takes
99 place at the interface between mature RCs. We also found that the number of RCs
100 correlates with nuclear size, suggesting a possible spatial restriction to the number of
101 viral genomes that initiate replication.

102 **Materials and methods**

103 **Cell culture**

104 African green monkey kidney cells (Vero, ATCC CCL-81) and human female
105 osteosarcoma cells (U2OS cells ATCC HTB-96) were grown in Dulbecco's Modified
106 Eagle Medium (DMEM X1; Gibco), supplemented with 10% Fetal Bovine Serum (FBS;
107 Gibco) and 1% Penicillin (10,000 units/ml) and Streptomycin (10 mg/ml; Biological
108 Industries, Israel).

109 **Viruses**

110 All viral recombinants are derivatives of herpes simplex type 1 strain 17. Each viral
111 recombinant contains one or two tag sequences for specific staining by FISH. To
112 facilitate isolation, both tag sequences are expression constructs for fluorescent
113 proteins. The red fluorescent protein mCherry driven by the human cytomegalovirus

114 promoter (CMVp) and the yellow fluorescent protein YPET driven by the simian virus
115 40 promoter (SV40p). Tag sequences were inserted into the viral genome by
116 homologous recombination. Viral DNA was co-transfected along with a plasmid
117 containing the tag sequences flanked by sequence homologies to the viral site of
118 insertion (synthetically generated by GenScript, Piscataway, NJ, USA). Recombinant
119 viruses were isolated from the progeny by plating lysate from transfected Vero cells
120 and picking fluorescent plaques using an epi-fluorescent microscope. Viral stocks
121 were prepared by growing purified plaques for each recombinant virus on Vero cells.
122 The viral recombinants were validated by PCR. Viral titers were measured by plaque
123 assay. An additional viral recombinant containing both tag sequences was isolated by
124 crossing the recombinant OK26 to the previously described OK11 (49) and selecting
125 for plaques containing two fluorescent proteins by plaque assay. All viral recombinants
126 constructed for this paper are described in Table 1

127 **Fluorescent probes**

128 A set of 20 fluorescent probes was designed to correspond to each one of the two tag
129 sequences. The probes for the CMVp:mCherry and sequences SV40p:YPET were
130 conjugated on their 5' end to the fluorescent dyes cy3 and cy5 respectively. An
131 additional probe was designed to stain HSV1 viral DNA non-specifically. This probe
132 corresponds to the viral a' sequence and conjugated to the fluorescent dye Alexa Fluor
133 488 on its 5' end. Fluorescent probes were synthesized by Integrated DNA
134 Technologies (Coralville, IA, USA). The probes were dissolved in TE buffer to a stock
135 concentration of 10 μM. Probes from each set were pooled together in equal ratios
136 and kept in -20^{0}C before hybridization. Probes sequences are detailed in Table 2.

137 **Fluorescent in situ hybridization**

138 Cells where seeded and grown to confluence inside 12 well plates underlined with a
139 glass coverslip. Cells were infected at MOI 20 with 200 µl inoculums. The cells were
140 incubated on ice for 1 hour following the addition of the inoculums. The inoculums
141 were then removed and replaced with DMEM+10%FBS. The infected cells were
142 incubated on 37°C for 6 hours. Medium was then removed and cells were washed with
143 PBS. Cells were then fixed with 1 ml 4% Paraformaldehyde (PFA) in PBSX0.3 for 10
144 minutes at room temperature. Cells were washed three times with 0.05% Triton X-100
145 in PBS at 5-minutes intervals. Cell nuclei were permeabilized by incubating the
146 coverslips with 0.5% Triton X-100 in PBS for 20 minutes. The 0.5% Triton was then
147 removed and 20% glycerol (Sigma-Aldrich) in PBS was added and incubated at room
148 temperature for 30-60 minutes. Following incubation, coverslips were repeatedly
149 frozen and thawed by dipping them in liquid nitrogen three times. Before refreezing,
150 the coverslips were dipped in the 20% glycerol solution to prevent cells from drying.
151 Coverslips were then washed with 0.05% Triton X-100 in PBS 3x5 minutes. Coverslips
152 were briefly washed in 0.1N HCl and incubated in fresh 0.1N HCl for 8 minutes.
153 Subsequently, the coverslips were washed with 0.05% Triton X-100 in PBS 3x5
154 minutes and then transferred to 50% formamide (Merck) in Saline Sodium Citrate
155 buffer X2 (SSCX2; diluted from SSCX20 prepared as follows: 175.3gr Sodium
156 Chloride (Bio-Lab), 88.2gr of Sodium Citrate (Merck) in 1 L of DDW, adjusted to pH
157 7.0 and filtrated). Viral genomes were hybridized using hybridization solution (10%
158 Dextran Sulfate (Calibochem) in SSCX2) containing the fluorescent probes (IDT; final
159 volume of 0.7 uM for each probe). For each coverslip, 5 µl of probe was placed on a
160 clean slide. Each slide was lifted out of the 50% formamide in SSCX2 solution and
161 coverslips were placed directly on the probe drop, cell side down and excess fluid was
162 removed. Rubber cement was applied to the edges of the coverslip to form a

163 temporary seal for hybridization. The slides were set aside to dry completely at room
164 temperature. The denaturing of cellular and probe DNA was achieved by placing the
165 slides on a hot slide block (Eppendorf) for precisely 2 minutes at 95°C. Following
166 denaturation, slides were sealed with parafilm and placed in a 37°C incubator for 72
167 hours. After sufficient hybridization, the rubber cement was removed from the slides.
168 Each coverslip was carefully removed and washed with SSCX2 3x5 minutes at 37°C
169 then washed with SSCX0.1 3x5 minutes at 63°C. For each coverslip, one drop of
170 Fluoroshield mounting medium containing DAPI (Abcam, Cambridge, MA, USA) was
171 placed on a fresh slide and each coverslip was placed cell side down on the drop.
172 Coverslips were sealed with nail polish. FISH protocol was adapted from (50).

173 **Microscopy**

174 Viral plaques were visualized under a Nikon Eclipse Ti-E epifluorescence inverted
175 microscope. Single cell analysis by FISH assay was performed using a Nikon Eclipse
176 Ti microscope equipped with Yokogawa CSU X-1 spinning disc confocal system.

177 **Image analysis**

178 Nuclei segmentation: Nuclei were automatically segmented from the DAPI channel as
179 follows. Gaussian smoothing (σ = 2) was applied to the image followed by Otsu
180 thresholding (51) to partition the image to nuclei / background regions. The nuclei
181 segmentation was refined by morphological operators: opening (width = 3 pixels) to
182 exclude small excesses; closing and an additional opening (width = 20 pixels) to unify
183 regions that belong to the same nucleus; Filling holes; considering only connected
184 regions of area exceeding 900 pixels - the minimal nucleus size. The output of this
185 stage is a set of masks, each corresponds to a single nucleus.

186 RC segmentation: RCs were segmented from each fluorescent channel independently.
187 Three groups of intensities were observed within each nucleus: background - at
188 intensities close to those outside the nucleus; intermediate - above the background
189 levels; and bright - which are the replication centers. First, Gaussian smoothing was
190 applied (σ = 2) to the image. Second, background statistics were calculated (mean
191 intensity, standard deviation) from the pixels outside the nuclei masks. A threshold of
192 2.5 standard deviations above the background mean intensity level was calculated.
193 To exclude pixels with background intensities from further analysis, the threshold was
194 applied for each nucleus mask. Otsu thresholding was then applied to the remaining
195 pixels, pixels below the threshold were pooled and a new threshold of two standard
196 deviations above the mean was calculated. The pixels above these thresholds were
197 defined as the RCs. The segmentation refined by applying morphological operators:
198 opening - excluding small excess, closing - filling gaps, and opening again -
199 disconnecting independent replication centers; all with a square kernel of 3 pixels
200 width. Last, were holes filled to define the RCs. Parameters were optimized by visual
201 assessment of RC segmentation accuracy.
202 Manual selection of nuclei: Region for statistical analysis were manually selected
203 based on the accurate segmentation of RCs. Regions of accurate RC segmentation
204 were selected independently for each channel, the intersection (implying accurate
205 segmentation on both channels) was used for quantifications.
206 The program outputs required measurements such as nuclei area, number and area
207 of RCs in each channel of each nucleus and the size of overlapping area for each RC.
208 The data were then transferred into Microsoft excel for subsequent processing. The
209 data were collected for each nucleus for further analysis. Cells without colocalization
210 were removed from further analysis. The ratio of colocalization area out of the total

211 area of RCs was calculated per cell (see supplementary excel file). Outliers were
212 removed using the interquartile method (1.5 times interquartile distance from either
213 the 1st of 3rd quartile). Two tails students T.test was performed to determine
214 significance.
215 Code availability: The Matlab source code used for analysis is publically available at
216 https://github.com/assafzar/RecombinationHSV1.

217 **Fluorescent plaque assay**

218 Cells (either Vero or U2OS) were grown to confluence in 12 well plates. Infection was
219 carried out at an MOI of 20 with a mix of the co-infecting viruses in 4°C. Cells were
220 harvested 9HPI. In Latrunculin B experiments, 1HPI the medium was replaced by
221 medium containing 2.5 μM Latrunculin B (Sigma). The infected cells were lysed by
222 freeze thawing and sonicating. The lysate was plated on 6 well plates containing Vero
223 cells. Following infection, cells were overlaid with growth medium containing 0.5%
224 methylcellulose and incubated for 48 hours. The plates were then inspected under
225 fluorescent microscope for plaque counting. The percent of dual color plaques out of
226 the total fluorescent plaques are indicated. A total of 8 wells, collected from two
227 individual plaque plating, from two technical repeats in two separate experiments,
228 were obtained. Modified Thompson Tau Test was used for outlier removal (no more
229 than one outlier per condition was detected). Two tails students T.test was performed
230 to determine significance.

231 **Results**

232 **A FISH based assay designed to detect inter-genomic recombination events**
233 **between co-infecting viruses.** Recombination among co-infecting HSV-1 strains is
234 a frequent event that can be detected by the progeny viruses released from infected
235 cells (8-10,12). To study the spatiotemporal constraints of these inter-genomic

236 recombination events we developed a FISH based experimental assay that enables
237 visualization of two different viral genomes within a co-infected nucleus. For this assay,
238 we constructed a series of viral isolates, isogenic to each other except for two unique
239 tag sequences. These tag sequences, YPET or mCherry encoding genes (yellow or
240 red fluorescent proteins, respectively) were inserted into various loci across the viral
241 genome (Figure 1A and Table 1). We designed two sets of fluorescent probes, one
242 set for each tag sequence (Figure 1B). Each probe set was conjugated to a distinct
243 fluorophore (Cy3 or Cy5) to enable visual identification of the genomes containing
244 each tag sequence. We hypothesize that using different mixtures of viruses should
245 lead to distinct patterns within the infected nucleus (Figure 1C). As was shown
246 previously for PRV (33), we expect that co-infection with two HSV-1 viruses containing
247 tag sequences at the same genomic locus cannot result in a new recombinant genome
248 containing both tags. Thus, each RC will react to a single fluorophore, including at the
249 contacting edges of proximate RCs (Figure 1C example I). Infection with a viral
250 recombinant containing two tag sequences within one genome is expected to result in
251 RCs stained with both fluorophores (dually-labelled RCs) (Figure 1C example IV).
252 Infection with two viral recombinants containing tag sequences at different genomic
253 loci could result in progeny genomes that either contain both tag sequences on a single
254 genome or contain neither tag sequence. One of two types of spatial patterns could
255 be expected to dominate under these conditions. Dually-labelled RCs (fully covered
256 by both probe sets) would imply that inter-genomic recombination takes place early
257 during infection before the viral DNA replicates and RCs mature. In this situation, the
258 reciprocal recombinant genome would contain no tag sequences and will generate
259 RCs that are not detected since they are not covered by any of the probes (Figure 1C
260 example II). Alternatively, partially overlapping RCs that fuse to each other at their

261 periphery, would suggest that inter-genomic recombination occurs later during the
262 infection cycle following viral DNA replication (Figure 1C example III). Therefore, this
263 FISH assay is designed to detect viral inter-genomic recombination events, with visual
264 readouts for when and where it takes place.

265 **Patterns of RC interactions dependent on HR.** To identify inter-genomic
266 recombination events, we co-infected Vero cells with different pairs of viruses listed in
267 Table 1, as detailed below. All infections were carried out at MOI 20, to increase the
268 likelihood of interactions between incoming viral genomes (8). Cells were either
269 infected with one virus that contained both mCherry and YPET tag sequences (OK31)
270 or were co-infected with two viruses, each carrying a different tag sequence (OK35
271 together with either OK25, OK32 or OK26). First, we collected the progeny viruses
272 released from the infected cells at 9 hours post infection (HPI) and plated them for
273 single plaques. We found that co-infections can result in dual color (yellow) plaques
274 under our different infection conditions (Figure 1D). The number of dual color plaques
275 was measured for each infection pair and compared to the total number of plaques
276 (Figure 1E). We found that the rate of dual color plaques was increased by ~5 fold for
277 infections with viral genomes carrying fluorescent protein genes at different genomic
278 sites when compared to infections with viruses where the genes are located at the
279 same genomic site. We note that there was no statistical difference between the two
280 infections with the viruses carrying the reporter genes at alternative sites in the
281 genomes (OK35 together with either OK32 or OK26). Our results corroborate the
282 conclusion that most progeny viruses containing dual color are the outcome of inter-
283 genomic HR events (8).

284 To visualize inter-genomic HR events at the single cell level, cells were co-infected
285 and fixed at 6HPI for hybridization with the appropriate fluorescent probes. Using

286 confocal fluorescent microscopy, we imaged the viral RCs and identified four distinct
287 patterns of interactions between the RCs (Figure 2A-D). The first interaction type (A -
288 minimal overlap) is of two RCs that come into close contact but without evidence of
289 mixing between the two RCs, i.e. no visible co-localized pixels and no intersection
290 between RCs margins (Figure 2A). These interactions were observed in all co-
291 infections, however they are significantly more pronounced when the tag sequences
292 were at the same relative genomic locus (OK25 and OK35, $P<0.05$, Figure 2E). The
293 second interaction type (B - periphery overlap) is of two RCs that come into close
294 contact and clearly mix with each other, as defined by the presence of dual color pixels
295 at the site of contact (Figure 2B). Note that the two channels do not necessarily co-
296 localize at the single pixel resolution at the contact sites (i.e., no yellow pixels), but do
297 co-localize at the region-scale. This was the most common interaction observed in all
298 co-infections (Figure 2E), with significantly increased frequency when the two tag
299 sequences were located at different sites of the viral genome: either OK26 and OK35
300 ($P<0.005$) or OK32 and OK35 ($P<0.05$). In the OK25 and OK35 dual infection (tags
301 located at the same genomic locus) this pattern cannot be due to HR, and in this case
302 reflects limitations of image resolution. In the third interaction type (C- Full overlap
303 within larger RC), a small RC (smaller than half the size of all other RCs in that nucleus)
304 is fully contained in a much larger RC (Figure 2C). This pattern was detected in about
305 5% of all co-infections (Figure 2E). The fourth interaction type (D – Full overlap) is a
306 dual color RC, in which the entire area of the RC contains both fluorophores (Figure
307 2D). The relative frequencies of these events can be quantitated during single or dual
308 infections (Figure 2E). As expected, the overlapping pattern accounted for ~ 90% of
309 RCs in cells with single infection of virus carrying both tag sequences (OK31), and in
310 about 3% of interactions in all dual co-infections. We deduce that our assay can be

311 used to readout inter-genomic recombination, since detectable HR events change the
312 overall distribution of the interactions among the RCs. In all co-infection assays, partial
313 overlaps at the point of contact are more frequent, compared to entirely overlapping
314 RCs. The rare occurrence of entirely overlapping RCs compared to the high frequency
315 of HR during HSV-1 co-infection (12) suggests that these RCs capture infrequent HR
316 events and cannot reflect the majority of HR between RCs. We therefore suggest that
317 inter-genomic HR occur at points of physical interaction between co-infecting genomes,
318 after viral DNA replication has initiated.

319 We have previously shown that infections of U2OS cells result in more HSV-1
320 genomes initiating gene expression per cell when compared to infections of Vero cells
321 (52). To test if the number of initiating genomes has an effect on the interactions
322 between RCs, we repeated our dual color infection assay in U2OS cells. Although
323 overall higher levels of dual-colored plaques were observed in U2OS cells when
324 compared to Vero cells, the relative levels of dual colored plaques attributed to HR (i.e
325 co-infection with either OK26 and OK35 or OK32 and OK35 relative to co-infection
326 with OK25 and OK35) was not different between the two cell types (Figure 1F). In both
327 U2OS and Vero cells there was no statistical difference between HR rates when
328 comparing infections with viruses that carry the second reporter gene at different
329 locations in the viral genome (OK26 versus OK32).

330 In FISH based experiments with infections of U2OS cells, we observed all four patterns
331 of RCs interactions that we defined for infections of Vero cells (Figure 3). However, in
332 U2OS cells, multiple RC interaction patterns in a single cell were more common than
333 in Vero cells (Figure 3A and 3B), probably due to the higher number of RCs observed
334 per cell in this cell type (see below, Figure 5A). The distribution of patterns observed
335 for the different infections in U2OS cells (Figure 3D) was similar to the distribution

336 detected in Vero cells (Figure 2E) although in U2OS cells lower rates of type C and D
337 interactions were observed in all co-infections tested.

338 **Overlap between RCs is enhanced by HR.** Merely identifying the patterns of overlap
339 does not estimate the relative proportion of the overlapping area between RCs.
340 Therefore, we developed a quantitative evaluation of the RC overlapping areas in each
341 cell. We found that common pixel based co-localization methods do not provide an
342 accurate estimate of the degree of overlap between HSV-1 RCs, probably due to the
343 relaxed form of the replicating viral DNA (34). Our results following infection with one
344 virus carrying the two tag sequences (OK31) showed limited co-localization at the pixel
345 level, similar to results obtained by two probes corresponding to adjacent loci on HSV-
346 1 genomes (53). We therefore applied a semi-automated object-based method to
347 quantify the degree of overlap for RCs in cells infected with viruses that have two
348 distinct genomes (see Methods). For each cell nucleus, we independently segmented
349 the RCs in each channel. The relative overlapping area was calculated as the ratio
350 between the overall area of the overlap and the total overall area occupied by viral
351 DNA (total area of all RCs minus the total overlap area). The images analysed were
352 collected from three infections carried out on different days from separate viral stocks.
353 Over 200 cells from each cell type were analysed for each co-infection. The dual-
354 tagged virus (OK31) allowed us to analyse fewer cells in this infection (N = 120 Vero,
355 N = 99 U2OS) but still with sufficient statistical power.

356 We analysed all the cells in which contacts between red and green RCs were observed
357 (more than 70% of cells in all co-infections). For both cell types, we found a small but
358 significant increase in the relative overlapping area in each nucleus for cells co-
359 infected by viruses with tags in different viral loci compared to cells co-infected by
360 viruses with tags in the same locus (greater than 16% increase for OK32 and OK35

361 infection on Vero cells and more than 30% increase in all other co-infections, Figure
362 4A-B). As with plaque assays (Figure 1E and F) and manual count (Figure 2E and 3D),
363 we did not observe significant differences in overlap between co-infections with viruses
364 that have tags in different loci. To confirm that cellular parameters do not bias our
365 measurements, we compared the relative overlapping area to the total nuclear area
366 (Figure 4C-D) or to the number of RCs per nucleus (not shown). We found no evidence
367 of correlation between these two parameters and the relative overlapping area in all
368 infection conditions (Pearson correlation bellow 0.3 for each of the infections). We
369 conclude that the observed significant increase in overlapping areas indicates the
370 readout of HR events. As mention above, the relative high background levels (OK25
371 and OK35 infection) of overlapping areas (~20%) are due in part to noise of the assay
372 and to non-HR events during viral replication.

373 **The number of RCs correlates with nuclear size.** We previously demonstrated that
374 the number of HSV-1 genomes replicating per cell can influence the outcome of
375 infection (54) and that host conditions prior to infection impact the outcome of infection
376 at the single cell level (54,55). To test the effect of cellular parameters on RC formation
377 and growth, we took advantage of our assay that provides an opportunity to quantitate
378 the number of mature RCs within individual cells as we can distinguish between the
379 colors of coalescing RCs. We note that OK31 infection was omitted from this analysis
380 due to our inability to distinguish between coalescing RCs in this infection. We
381 therefore tested association of the number of RCs to other parameters of the infected
382 cell. First, we observed that in U2OS cells more RCs were detected per individual
383 nucleus than in Vero cells. We detected an average of ~5.1 RCs per nucleus in U2OS
384 cells compared to ~3.7 RCs per nucleus in Vero cells (1.375 fold increase, Figure 5A).
385 Interestingly, a similar fold increase of ~1.38 was identified in nuclear area (Figure 5B).

386 This led us to speculate that nuclear area may correlate with the number of RCs per
387 nucleus. Indeed, the number of RCs correlates to the nuclear area for individual cells
388 in each of the cell types (Pearson correlation: $R > 0.538$ for all co-infections, $p < 0.0001$
389 for all co-infections, Figure 5C-D). We hypothesize that the increase in the number of
390 RCs per nucleus will result in more total viral DNA (RCs area) in larger nuclei. As
391 expected, the nuclear area correlates with the total area of the RCs per nucleus
392 (Pearson correlation: $R = 0.530$ for OK32 and OK35 co-infection on Vero and $R >$
393 0.625 for all other co-infections, $p < 0.0001$ for all co-infections, Figure 5E-F). We
394 speculated that the increase in total RCs area could also result from the possibility that
395 RCs expand faster to a larger size in larger nuclei. We therefore compared the mean
396 RC area (per cell) to the total nuclear area (Figure 5G-H). We found a much weaker
397 correlation between these parameters (Pearson correlation: < 0.5 for U20S cells and
398 < 0.3 for Vero cells in each of the infections). These results suggest that the increase
399 in RC area in larger nuclei results from higher numbers of RCs rather than increased
400 RC size. Taken together, our results suggest that nuclear size could be a restricting
401 factor, limiting the number of incoming genomes that are able to initiate replication.

402 **Inhibition of RC movement reduces the rate of HR events.** It was previously shown
403 that RC movement towards each other relies upon the formation of actin filaments (31).
404 Since our results suggest that HR events occur between coalescing RCs, we tested
405 whether disruption of RC movement will result in reduction in recombination rates. We
406 treated co-infected cells with latrunculin B, an inhibitor of actin polymerization, and
407 tested for recombination rate among the progeny viruses by fluorescent plaque assay.
408 Vero and U2OS cells were infected with the pairs of viral constructs that produce dual
409 color progeny as a result of HR (OK32 and OK35, OK26 andOK35) and were treated
410 with latrunculin B. At 9HPI, progeny viruses were collected and plated for single

411 plaques. The rate of HR events was compared to the progeny from infection with the
412 pair of viral constructs carrying the fluorescent gene at the same site (OK25 and OK35).
413 We note that treatment with latrunculin B increased the level of dual colored plaques
414 that did not result for HR (from the viral pair OK25 and OK35) compared to untreated
415 cells (Figure 6). To estimate the rate of HR for viral pairs with fluorescent tags in
416 different loci of the viral genome, the average rate of OK25 and OK35 dual colored
417 plaques was subtracted from the total rate of dual colored plaques from the viral pairs
418 OK35 and either OK26 or OK32. The presence of latrunculin B reduced HR rates
419 compared to untreated cells for both infection pairs in both cell types (Figure 6).
420 Statistically significant decreases were observed in both cells during OK26 and OK35
421 co-infection and only in U2OS cells for OK32 and OK35 co-infection. These results
422 suggest that RC movement enhances inter-genomic HR, corroborating our initial
423 conclusion that HR events occur at the contact point of coalescing RCs.

424 **Triple-color FISH indicates that inter-genomic recombination occurs at edge of**
425 **coalescing RCs.** We speculated that if there are RCs that originate from a single
426 recombinant genome and contain both tag sequences, there must be reciprocal
427 recombinant RCs that contain none of the tags and are undetectable in our FISH assay
428 (Figure 1C II). To determine whether these RCs exist, we designed an additional
429 probe conjugated to a third fluorophore corresponding to the genomic HSV a'
430 sequence, a repetitive sequence found in four copies within the HSV-1 genome (56),
431 This probe stains all HSV-1 viral DNA regardless of the tag sequence inserted. Both
432 Vero and U2OS cells were co-infected with two isolates containing tags at different
433 genomic loci, fixed and hybridized to all three probes as previously described. We
434 inspected over 600 RCs from each cell type and found that 99.6% stained by the HSV
435 non-specific probes reacted to either of the two specific probe sets (example in Figure

436 7). The existence of at least one tag sequence for all RCs suggests that RCs are not
437 generated from recombinant genomes. This result further supports the hypothesis that
438 recombination occurs at the edge of mature coalescing RCs at later stages of infection
439 and is coupled with replication. Similarly, all coalescing areas between mature RCs
440 respond to both the specific probe sets in contrast to our prediction that half of these
441 areas should not respond to either specific probe (Figure 1C III). This finding suggests
442 that these sites of recombination contain a mixture of genomes that contain either both
443 tags or none of them. We therefore hypothesize that these sites of recombination do
444 not arise from a single recombination event (since this would have led to the
445 phenomenon of both tags or none) but rather from multiple events along the contact
446 front of replicating RCs.

447 Discussion

448 Recombination among co-infecting herpesviruses is fundamentally important for
449 understanding viral evolution and pathogenesis (5). It is also important to consider
450 inter-genomic recombination when developing vectors for vaccination and oncolytic
451 viral therapy, since evidence for recombination between a vaccine strain and a wild
452 type strain has already been found in herpesviruses (57). Here, we developed a
453 unique experimental system to identify the spatiotemporal constraints of inter-genomic
454 recombination. Our results corroborate the hypothesis that each RC initiates from a
455 single incoming genome. We visualized HR increasing in the overlapping areas
456 between RCs, although the experimental system also detects overlapping signals
457 unrelated to HR. We found that most viral inter-genomic recombination events that we
458 detected occur at the edges of developing RCs where they coalesce with others.
459 Inhibition of RCs movement reduced the rate of recombination, further corroborating

460 that HR events occur after coalescencing of RCs. Finally, we suggest that areas in
461 which overlapping RCs are detected result from multiple independent recombination
462 events.

463 We have infected cells with different combinations of viral isolates: OK35 & OK25
464 where tags are inserted into the same genomic locus, OK35 & OK32 containing tags
465 on separate genomic loci spaced approximately 72 Kbp apart, and OK35 & OK26
466 where they are spaced approximately 105 Kbp apart. In our analysis, we have not
467 detected any significant differences between the two combinations of viruses tagged
468 at separate genomic loci (i.e. OK35 & OK32 and OK35 & OK26). This supports the
469 hypothesis that recombination events occur between replicating genomes that are in
470 either branched or circular concatemeric states (7). Since HSV-1 maintains the 4
471 genome isomers at equivalent distributions (58), the 105Kbp distance between the
472 markers is actually ~50Kbp in half of the concatemeric forms. This may explain the
473 inability to distinguish differences in recombination rates when the markers are not
474 closely linked, as previously suggested (7).

475 We observed four recognizable patterns of interactions between adjacent RCs: i. no
476 mixing, ii. partial mixing, iii. one within another and iv. complete overlap (Figure 2 and
477 3). From our previous results with PRV (33), we expected that the lack of mixing of
478 RCs would be the dominant interaction following co-infection with two viruses carrying
479 tag sequences at the same location in the viral genomes (OK25 and OK35). We found
480 that this readout is most commonly observed in this co-infection, although to our
481 surprise the majority of RCs (~60%) showed some degree of mixing. Revisiting the
482 images obtained during the Kobiler *et al.* paper (33) suggested that there is no major
483 difference between the images from the two alphaherpesviruses co-infection. i.e the
484 overlap between signals was also observed in the PRV experiments, but was

485 attributed to image resolution and noise. We note that robust quantitative analysis of
486 PRV images was not carried out.

487 The partial mixing of RCs was the most common interaction observed among the
488 different co-infection conditions tested (Figure 2E). This is in part due to the
489 categorization of all partial mixing interactions into one single pattern, regardless of
490 the proportion of mixing. To overcome this problem, we developed an image analysis
491 code that calculates the relative area of mixing. We found a significant increase in the
492 relative area of mixing when co-infections were carried out with viruses in which HR
493 can result in the mixing of the colors. These measurements were significant both at
494 the single cell level (Figure 4A and B) and at the single RC level, indicating that a
495 significant proportion of the mixing we observe is due to HR. On the other hand, even
496 when HR cannot allow for signal mixing (i.e. OK25 and OK35 co-infection), we
497 observed RCs and cells in which a high proportion of mixing occurred (Figure 4E and
498 F). Similar findings were found in PRV co-infection assays (33). These results suggest
499 that some color mixing can occur without recombining both tag sequences into the
500 same genome. Alternatively they could reflect non-HR events during replication, which
501 were previously observed both in HSV-1 replication (58) and in other herpesviruses
502 (59). These explanations are not mutually exclusive, and both may contribute to the
503 mixing of colors observed without HR.

504 The interaction in which one RC is fully mixed into a larger RC (Figure 2C) can be
505 explained by multiple mechanisms. First, it could originate from a small RC that
506 coalesces with a larger one. Second, the smaller RC could interact with two larger
507 RCs that flank both sides of the small RC and eventually unite into a single larger RC.
508 A third mechanism could involve the recently observed condensed viral genomes at
509 the edge of RCs (34). Sekine *et al.* showed that at 3HPI several incoming genomes

510 remain condensed at the periphery of an enlarging RC (34). These condensed
511 genomes might be silent throughout the lytic infection or may serve as templates for
512 recombination at later time points (which will result in our observed third interaction).
513 The latter hypothesis fits our finding that this interaction is less frequent in U2OS
514 (Figure 2E and 3D). Since U2OS cells lack ATRX and has compromised expression
515 of other intrinsic immunity proteins (60-62), they are less likely to silence incoming
516 genomes (52), and we speculate that they may have lower amounts of condensed
517 genomes. Further experiments are required to distinguish between these different
518 possibilities.

519 Our experimental system provides the opportunity to calculate accurately the number
520 of functional RCs within a nucleus, since the separation by color increases our ability
521 to differentiate between coalesced RCs. We were able to detect an increase in the
522 average number of RCs detected in U2OS nuclei compared to Vero nuclei. This
523 corroborates our previous finding that in U2OS cells on average a higher number of
524 incoming viral genomes per cell initiate expression and replication compared to Vero
525 cells (52). These observations also further support the emerging view that individual
526 RCs initiate from single incoming genomes (33).

527 We define correlations between the nuclear area and the number of detectable RCs
528 both in Vero and U2OS cells, similar to the correlation between cell size (as measured
529 by flow cytometry) and the number of replicating genomes (54). Since our images
530 represent snapshots during the infection process, we cannot distinguish between the
531 possibilities that larger nuclei allow a larger number of incoming viral genomes to
532 initiate replication or that the nuclei in which more genomes initiated replication expand
533 faster. The use of new methods to visualise incoming genomes using click chemistry
534 (34,35,63) should be able to resolve these two alternatives.

535 We note that U2OS cells are known to have larger nuclei and indeed have more RCs
536 per cell than Vero cells. Similarly, HeLa cells that are relatively small cells with small
537 nuclei have fewer incoming HSV-1 genomes that initiate replication (54). However,
538 both U2OS and HeLa cells originated from tumors and carry multiple abnormalities
539 that might regulate the number of herpes genomes that initiate replication. We are not
540 certain that average nuclear size of a cell type is a main factor in determining the
541 number of herpes genomes initiating replication among cell types.

542 Our analysis of the dual color FISH experiments led us to hypothesise that most viral
543 inter-genomic HR events occur at the edge of the RCs and only after they coalesce.
544 Further support for this hypothesis was obtained from the latrunculin experiment.
545 Since viral RCs movement in the nucleus is dependent of actin filaments (31), the
546 inhibition of actin polymerisation by the latrunculin B inhibitor should reduce RCs
547 coalescence. Thus, the reduction in inter-genomic HR rates observed with latrunculin
548 treatment can be attributed to a reduction in interaction between growing RCs. We
549 note that when RCs enlarge, eventually, they will probably interact with each other
550 without direct motion.

551 In mammalian nuclei, translocations between chromosomes, that can lead to
552 tumorgenicity and other illnesses, are thought to occur among adjacent chromosomes
553 (64,65). Our results support the requirement of proximity (contact first) among DNA
554 molecules prior to recombination. Thus, maintaining genome integrity may require
555 physical separation between DNA molecules. It will be interesting to determine what
556 defines the location of viral replication compartments and the extent to which liquid
557 phase separation (66) and other mechanisms regulate their mingling.

558 In conclusion, our results support a model in which incoming viral genomes establish
559 RCs at distinct sites in the nucleus. The vast majority of RCs initiate from a single
560 genome and only at later stages coalesce but maintain a detectable separation
561 between RCs. These areas of interactions between the expanding RCs are predicted
562 to be the site in which HR occurs in tight association with viral DNA replication. Our
563 results suggest that in these sites, inter-genomic recombination is a frequent event,
564 although not all areas of interactions between the RCs are supportive of close contact
565 that can lead to recombination. Further research will shed light on the differences
566 between these types of RC interactions.

567

Funding

This work was supported by grants from the Israel Science foundation (grant #1387/14) to O.K., the EU CIG grant (FP7-2012-333653) to O.K., the National Institute of Health (NS082240) to M.D.W., the United States - Israel Binational Science Foundation (grant # 2015395) to O.K. and M.D.W., and a Marguerite Stolz Research Fellowship to O.K. E.T. is supported by the Buchman Scholarship and A.Z. was supported by the National Institute of Health Grant to Gaudenz Danuser (P01 GM103723). The funders had no role in study design, data collection and analysis, decision to publish, or preparation of the manuscript.

Acknowledgement

We thank Eitan Erez Zahavi, Ariel Ionescu and Eran Perlson for advice and valuable support and all Kobiler lab members for their comments.

References

1. Muller, H.J. (1964) The Relation of Recombination to Mutational Advance. *Mutat Res*, **106**, 2-9.
2. Felsenstein, J. (1974) The evolutionary advantage of recombination. *Genetics*, **78**, 737-756.
3. Sanjuan, R. and Domingo-Calap, P. (2016) Mechanisms of viral mutation. *Cell Mol Life Sci*, **73**, 4433-4448.
4. Holmes, E.C. (2008) Evolutionary history and phylogeography of human viruses. *Annu Rev Microbiol*, **62**, 307-328.
5. Renner, D.W. and Szpara, M.L. (2017) The Impacts of Genome-wide Analyses on our Understanding of Human Herpesvirus Diversity and Evolution. *J Virol*.
6. Brown, S.M., Ritchie, D.A. and Subak-Sharpe, J.H. (1973) Genetic studies with herpes simplex virus type 1. The isolation of temperature-sensitive mutants, their arrangement into complementation groups and recombination analysis leading to a linkage map. *J Gen Virol*, **18**, 329-346.
7. Honess, R.W., Buchan, A., Halliburton, I.W. and Watson, D.H. (1980) Recombination and linkage between structural and regulatory genes of herpes simplex virus type 1: study of the functional organization of the genome. *J Virol*, **34**, 716-742.
8. Law, G.A., Herr, A.E., Cwick, J.P. and Taylor, M.P. (2018) A New Approach to Assessing HSV-1 Recombination during Intercellular Spread. *Viruses*, **10**.

600 9. Lee, K., Kolb, A.W., Sverchkov, Y., Cuellar, J.A., Craven, M. and Brandt, C.R. (2015)
601 Recombination Analysis of Herpes Simplex Virus 1 Reveals a Bias toward GC Content and the
602 Inverted Repeat Regions. *J Virol*, **89**, 7214-7223.
603 10. Morse, L.S., Buchman, T.G., Roizman, B. and Schaffer, P.A. (1977) Anatomy of herpes simplex
604 virus DNA. IX. Apparent exclusion of some parental DNA arrangements in the generation of
605 intertypic (HSV-1 X HSV-2) recombinants. *J Virol*, **24**, 231-248.
606 11. Schaffer, P.A., Aron, G.M., Biswal, N. and Benyesh-Melnick, M. (1973) Temperature-sensitive
607 mutants of herpes simplex virus type 1: isolation, complementation and partial
608 characterization. *Virology*, **52**, 57-71.
609 12. Tang, K.W., Norberg, P., Holmudden, M., Elias, P. and Liljeqvist, J.A. (2014) Rad51 and Rad52
610 are involved in homologous recombination of replicating herpes simplex virus DNA. *PLoS*
611 *One*, **9**, e111584.
612 13. Szpara, M.L., Gatherer, D., Ochoa, A., Greenbaum, B., Dolan, A., Bowden, R.J., Enquist, L.W.,
613 Legendre, M. and Davison, A.J. (2014) Evolution and diversity in human herpes simplex virus
614 genomes. *J Virol*, **88**, 1209-1227.
615 14. Kolb, A.W., Ane, C. and Brandt, C.R. (2013) Using HSV-1 genome phylogenetics to track past
616 human migrations. *PLoS One*, **8**, e76267.
617 15. Bowden, R., Sakaoka, H., Donnelly, P. and Ward, R. (2004) High recombination rate in herpes
618 simplex virus type 1 natural populations suggests significant co-infection. *Infect Genet Evol*,
619 **4**, 115-123.
620 16. Kobiler, O., Drayman, N., Butin-Israeli, V. and Oppenheim, A. (2012) Virus strategies for
621 passing the nuclear envelope barrier. *Nucleus*, **3**, 526-539.
622 17. Burkham, J., Coen, D.M. and Weller, S.K. (1998) ND10 protein PML is recruited to herpes
623 simplex virus type 1 prereplicative sites and replication compartments in the presence of
624 viral DNA polymerase. *J Virol*, **72**, 10100-10107.
625 18. Dembowski, J.A. and DeLuca, N.A. (2015) Selective recruitment of nuclear factors to
626 productively replicating herpes simplex virus genomes. *PLoS Pathog*, **11**, e1004939.
627 19. Lilley, C.E., Chaurushiya, M.S., Boutell, C., Everett, R.D. and Weitzman, M.D. (2011) The
628 intrinsic antiviral defense to incoming HSV-1 genomes includes specific DNA repair proteins
629 and is counteracted by the viral protein ICP0. *PLoS Pathog*, **7**, e1002084.
630 20. Liptak, L.M., Uprichard, S.L. and Knipe, D.M. (1996) Functional order of assembly of herpes
631 simplex virus DNA replication proteins into prereplicative site structures. *J Virol*, **70**, 1759-
632 1767.
633 21. Mohni, K.N., Livingston, C.M., Cortez, D. and Weller, S.K. (2010) ATR and ATRIP are recruited
634 to herpes simplex virus type 1 replication compartments even though ATR signaling is
635 disabled. *J Virol*, **84**, 12152-12164.
636 22. Reyes, E.D., Kulej, K., Pancholi, N.J., Akhtar, L.N., Avgousti, D.C., Kim, E.T., Bricker, D.K.,
637 Spruce, L.A., Koniski, S.A., Seeholzer, S.H. *et al.* (2017) Identifying Host Factors Associated
638 with DNA Replicated During Virus Infection. *Mol Cell Proteomics*, **16**, 2079-2097.
639 23. Taylor, T.J. and Knipe, D.M. (2004) Proteomics of herpes simplex virus replication
640 compartments: association of cellular DNA replication, repair, recombination, and chromatin
641 remodeling proteins with ICP8. *J Virol*, **78**, 5856-5866.
642 24. Vogel, J.L. and Kristie, T.M. (2013) The dynamics of HCF-1 modulation of herpes simplex virus
643 chromatin during initiation of infection. *Viruses*, **5**, 1272-1291.
644 25. Zhong, L. and Hayward, G.S. (1997) Assembly of complete, functionally active herpes simplex
645 virus DNA replication compartments and recruitment of associated viral and cellular proteins
646 in transient cotransfection assays. *J Virol*, **71**, 3146-3160.
647 26. Roizman, B. and Zhou, G. (2015) The 3 facets of regulation of herpes simplex virus gene
648 expression: A critical inquiry. *Virology*, **479-480**, 562-567.

649 27. Quinlan, M.P., Chen, L.B. and Knipe, D.M. (1984) The intranuclear location of a herpes
650 simplex virus DNA-binding protein is determined by the status of viral DNA replication. *Cell*,
651 **36**, 857-868.
652 28. de Bruyn Kops, A. and Knipe, D.M. (1988) Formation of DNA replication structures in herpes
653 virus-infected cells requires a viral DNA binding protein. *Cell*, **55**, 857-868.
654 29. Lukonis, C.J. and Weller, S.K. (1996) Characterization of nuclear structures in cells infected
655 with herpes simplex virus type 1 in the absence of viral DNA replication. *J Virol*, **70**, 1751-
656 1758.
657 30. Taylor, T.J., McNamee, E.E., Day, C. and Knipe, D.M. (2003) Herpes simplex virus replication
658 compartments can form by coalescence of smaller compartments. *Virology*, **309**, 232-247.
659 31. Chang, L., Godinez, W.J., Kim, I.H., Tektonidis, M., de Lanerolle, P., Eils, R., Rohr, K. and
660 Knipe, D.M. (2011) Herpesviral replication compartments move and coalesce at nuclear
661 speckles to enhance export of viral late mRNA. *Proc Natl Acad Sci U S A*, **108**, E136-144.
662 32. Sourvinos, G. and Everett, R.D. (2002) Visualization of parental HSV-1 genomes and
663 replication compartments in association with ND10 in live infected cells. *The EMBO journal*,
664 **21**, 4989-4997.
665 33. Kobiler, O., Brodersen, P., Taylor, M.P., Ludmir, E.B. and Enquist, L.W. (2011) Herpesvirus
666 replication compartments originate with single incoming viral genomes. *MBio*, **2**.
667 34. Sekine, E., Schmidt, N., Gaboriau, D. and O'Hare, P. (2017) Spatiotemporal dynamics of HSV
668 genome nuclear entry and compaction state transitions using bioorthogonal chemistry and
669 super-resolution microscopy. *PLoS Pathog*, **13**, e1006721.
670 35. Dembowski, J.A. and DeLuca, N.A. (2018) Temporal Viral Genome-Protein Interactions
671 Define Distinct Stages of Productive Herpesviral Infection. *MBio*, **9**.
672 36. Reuven, N.B., Staire, A.E., Myers, R.S. and Weller, S.K. (2003) The herpes simplex virus type 1
673 alkaline nuclease and single-stranded DNA binding protein mediate strand exchange in vitro.
674 *J Virol*, **77**, 7425-7433.
675 37. Schumacher, A.J., Mohni, K.N., Kan, Y.N., Hendrickson, E.A., Stark, J.M. and Weller, S.K.
676 (2012) The HSV-1 Exonuclease, UL12, Stimulates Recombination by a Single Strand Annealing
677 Mechanism. *Plos Pathogens*, **8**.
678 38. Weller, S.K. and Coen, D.M. (2012) Herpes Simplex Viruses: Mechanisms of DNA Replication.
679 *Csh Perspect Biol*, **4**.
680 39. Advani, S.J., Weichselbaum, R.R. and Roizman, B. (2003) Herpes simplex virus 1 activates
681 cdc2 to recruit topoisomerase II alpha for post-DNA synthesis expression of late genes. *Proc*
682 *Natl Acad Sci U S A*, **100**, 4825-4830.
683 40. Edwards, T.G., Bloom, D.C. and Fisher, C. (2018) The ATM and Rad3-Related (ATR) Protein
684 Kinase Pathway Is Activated by Herpes Simplex Virus 1 and Required for Efficient Viral
685 Replication. *J Virol*, **92**.
686 41. Lilley, C.E., Carson, C.T., Muotri, A.R., Gage, F.H. and Weitzman, M.D. (2005) DNA repair
687 proteins affect the lifecycle of herpes simplex virus 1. *Proc Natl Acad Sci U S A*, **102**, 5844-
688 5849.
689 42. Mohni, K.N., Dee, A.R., Smith, S., Schumacher, A.J. and Weller, S.K. (2013) Efficient herpes
690 simplex virus 1 replication requires cellular ATR pathway proteins. *J Virol*, **87**, 531-542.
691 43. De Chiara, G., Racaniello, M., Mollinari, C., Marcocci, M.E., Aversa, G., Cardinale, A.,
692 Giovanetti, A., Garaci, E., Palamara, A.T. and Merlo, D. (2016) Herpes Simplex Virus-Type1
693 (HSV-1) Impairs DNA Repair in Cortical Neurons. *Front Aging Neurosci*, **8**, 242.
694 44. Parkinson, J., Lees-Miller, S.P. and Everett, R.D. (1999) Herpes simplex virus type 1
695 immediate-early protein vmw110 induces the proteasome-dependent degradation of the
696 catalytic subunit of DNA-dependent protein kinase. *J Virol*, **73**, 650-657.
697 45. Smith, S., Reuven, N., Mohni, K.N., Schumacher, A.J. and Weller, S.K. (2014) Structure of the
698 herpes simplex virus 1 genome: manipulation of nicks and gaps can abrogate infectivity and
699 alter the cellular DNA damage response. *J Virol*, **88**, 10146-10156.

700 46. Smith, S. and Weller, S.K. (2015) HSV-I and the cellular DNA damage response. *Future Virol*,
701 **10**, 383-397.
702 47. Trigg, B.J., Lauer, K.B., Fernandes Dos Santos, P., Coleman, H., Balmus, G., Mansur, D.S. and
703 Ferguson, B.J. (2017) The Non-Homologous End Joining Protein PAXX Acts to Restrict HSV-1
704 Infection. *Viruses*, **9**.
705 48. Wilkinson, D.E. and Weller, S.K. (2006) Herpes simplex virus type I disrupts the ATR-
706 dependent DNA-damage response during lytic infection. *J Cell Sci*, **119**, 2695-2703.
707 49. Taylor, M.P., Kobiler, O. and Enquist, L.W. (2012) Alphaherpesvirus axon-to-cell spread
708 involves limited virion transmission. *Proc Natl Acad Sci U S A*, **109**, 17046-17051.
709 50. Cremer, M., Grasser, F., Lanctot, C., Muller, S., Neusser, M., Zinner, R., Solovei, I. and
710 Cremer, T. (2008) Multicolor 3D fluorescence in situ hybridization for imaging interphase
711 chromosomes. *Methods Mol Biol*, **463**, 205-239.
712 51. Otsu, N. (1979) Threshold Selection Method from Gray-Level Histograms. *Ieee T Syst Man*
713 *Cyb*, **9**, 62-66.
714 52. Shapira, L., Ralph, M., Tomer, E., Cohen, S. and Kobiler, O. (2016) Histone Deacetylase
715 Inhibitors Reduce the Number of Herpes Simplex Virus-1 Genomes Initiating Expression in
716 Individual Cells. *Front Microbiol*, **7**, 1970.
717 53. Li, Z., Fang, C., Su, Y., Liu, H., Lang, F., Li, X., Chen, G., Lu, D. and Zhou, J. (2016) Visualizing
718 the replicating HSV-1 virus using STED super-resolution microscopy. *Virol J*, **13**, 65.
719 54. Cohen, E.M. and Kobiler, O. (2016) Gene Expression Correlates with the Number of Herpes
720 Viral Genomes Initiating Infection in Single Cells. *PLoS Pathog*, **12**, e1006082.
721 55. Drayman, N., Karin, O., Mayo, A., Danon, T., Shapira, L., Rafael, D., Zimmer, A., Bren, A.,
722 Kobiler, O. and Alon, U. (2017) Dynamic Proteomics of Herpes Simplex Virus Infection. *MBio*,
723 **8**.
724 56. Hayward, G.S., Jacob, R.J., Wadsworth, S.C. and Roizman, B. (1975) Anatomy of herpes
725 simplex virus DNA: evidence for four populations of molecules that differ in the relative
726 orientations of their long and short components. *Proc Natl Acad Sci U S A*, **72**, 4243-4247.
727 57. Lee, S.W., Markham, P.F., Coppo, M.J., Legione, A.R., Markham, J.F., Noormohammadi, A.H.,
728 Browning, G.F., Ficorilli, N., Hartley, C.A. and Devlin, J.M. (2012) Attenuated vaccines can
729 recombine to form virulent field viruses. *Science*, **337**, 188.
730 58. Mahiet, C., Ergani, A., Huot, N., Alende, N., Azough, A., Salvaire, F., Bensimon, A., Conseiller,
731 E., Wain-Hobson, S., Labetoulle, M. *et al.* (2012) Structural variability of the herpes simplex
732 virus 1 genome in vitro and in vivo. *J Virol*, **86**, 8592-8601.
733 59. Rijsewijk, F.A., Verschuren, S.B., Madic, J., Ruuls, R.C., Renaud, P. and van Oirschot, J.T.
734 (1999) Spontaneous BHV1 recombinants in which the gI/gE/US9 region is replaced by a
735 duplication/inversion of the US1.5/US2 region. *Arch Virol*, **144**, 1527-1537.
736 60. Heaphy, C.M., de Wilde, R.F., Jiao, Y., Klein, A.P., Edil, B.H., Shi, C., Bettegowda, C.,
737 Rodriguez, F.J., Eberhart, C.G., Hebbar, S. *et al.* (2011) Altered telomeres in tumors with
738 ATRX and DAXX mutations. *Science*, **333**, 425.
739 61. Hancock, M.H., Corcoran, J.A. and Smiley, J.R. (2006) Herpes simplex virus regulatory
740 proteins VP16 and ICP0 counteract an innate intranuclear barrier to viral gene expression.
741 *Virology*, **352**, 237-252.
742 62. Yao, F. and Schaffer, P.A. (1995) An activity specified by the osteosarcoma line U2OS can
743 substitute functionally for ICP0, a major regulatory protein of herpes simplex virus type 1. *J*
744 *Virol*, **69**, 6249-6258.
745 63. Alandijany, T., Roberts, A.P.E., Conn, K.L., Loney, C., McFarlane, S., Orr, A. and Boutell, C.
746 (2018) Distinct temporal roles for the promyelocytic leukaemia (PML) protein in the
747 sequential regulation of intracellular host immunity to HSV-1 infection. *PLoS Pathog*, **14**,
748 e1006769.
749 64. McCord, R.P. and Balajee, A. (2018) 3D Genome Organization Influences the Chromosome
750 Translocation Pattern. *Adv Exp Med Biol*, **1044**, 113-133.

751 65. Misteli, T. and Soutoglou, E. (2009) The emerging role of nuclear architecture in DNA repair
752 and genome maintenance. *Nat Rev Mol Cell Biol*, **10**, 243-254.
753 66. McSwiggen, D.T., Hansen, A.S., Marie-Nelly, H., Teves, S., Heckert, A., Dugast-Darzacq, C.,
754 Hao, Y., Umemoto, K.K., Tjian, R. and Darzacq, X. (2018) Transient DNA Binding Induces RNA
755 Polymerase II Compartmentalization During Herpesviral Infection Distinct From Phase
756 Separation. *bioRxiv*.

757 # Figure legends

758 **Figure 1. Schematic representation of dual colour FISH assay**. **(A)** A series of viral
759 recombinants with two unique tag sequences (designated red and green) inserted into various
760 loci of the parental genome. Illustration of the insertion sequences (colour boxes) and viral
761 genomes (black line with repeats marked in gray boxes). Illustrations are not to scale. **(B)** Two
762 sets of probes conjugated to distinct fluorophores, each set corresponds to one tag sequence.
763 **(C)** Illustration of expected results, in which the gray nucleus contains viral RCs originating
764 from genomes with either one tag sequences (red or green), two tag sequences (yellow) or
765 no tag sequence (black). The expected results in the case of infection with tag sequences on
766 the same locus of two co-infecting genomes **(I)**, with tag sequences on separate loci in two
767 co-infected genomes where recombination takes place before DNA replication **(II)** or following
768 DNA replication **(III)** and with two tag sequences in the same genome **(IV)**. **(D)** Representative
769 images of viral plaques initiating from progeny viruses collected from Vero cells co-infected
770 with different viral recombinants as marked above each image. Scale bar is 100 µm. **(E-F)**
771 Progeny viruses from either Vero **(E)** or U2OS **(F)** cells co-infected with the viral recombinants
772 OK35 & OK25 (blue), OK35 & OK32 (yellow) and OK35 & OK26 (orange) were plated for
773 individual plaques and colors quantitated. The percent of dual color plaques are indicated.
774 The averages are shown from two individual plaque plating, from two technical repeats in two
775 separate experiments. Error bars represent standard error of the means. ***$P < 0.001$; by t
776 test.

777 **Figure 2. Observed patterns of RC interactions. (A-D)** Representative images of Vero cells
778 infected with viral isolates containing two genomic tags, each corresponding to a set of
779 fluorescent probes. The probe sets are imaged separately in red and green (I and II) and
780 merged (III). Four observed patterns of interaction between RCs are represented: **(A)** RCs
781 containing different tag sequences come into contact without overlap (orange arrowhead),
782 imaged from cells infected by two viral recombinants containing tag sequences on the same
783 genomic locus (OK25 and OK35). **(B)** RCs containing different tag sequences overlap at their
784 periphery (white arrowhead), imaged from cells infected with two viral recombinants containing
785 tag sequences on separate genomic loci (OK32 and OK35). **(C)** RC containing one tag
786 sequence overlap completely within a larger RC with the second tag (black arrowhead) imaged

787 from cells infected with two viral recombinants containing tag sequences on separate genomic
788 loci (OK26 and OK35). **(D)** Entirely overlapping RCs, imaged from cells infected by a viral
789 recombinant containing two tag sequences on the same genome in separate loci (OK31).
790 DAPI nuclear stain is presented in gray. Scale bar is 5µm. **(E)** Percent of each of the observed
791 RCs interactions (A to D) from the total number of RCs interactions. Manually counted at the
792 different co-infection conditions. >70 RCs interactions per infection type per experiment were
793 counted. An average of three experiments and the standard deviation in brackets are shown.

794 **Figure 3. Patterns of RC interactions on U2OS cells. (A-C)** Representative images of
795 U2OS cells infected with either **(A)** OK25 and OK35, **(B)** OK32 and OK35 or **(C)** OK31 viral
796 recombinants. The probe sets are imaged separately in red and green (I and II) and merged
797 (III). Arrowheads are colour coded as in figure 2. DAPI is presented in gray. Scale bar is 5µm.
798 (**D**) Percent of each of the observed RCs interactions out of total RCs interactions. Manually
799 counted at the different co-infection conditions. >70 RCs interactions per infection type per
800 experiment were counted. An average of three experiments and the standard deviation in
801 brackets are shown.

802 **Figure 4. HR enhances overlap between viral genomes.** Vero cells **(A, C)** and U2OS cells
803 **(B, D)** were infected with the viral isolates OK35 & OK25 where tags are inserted into the
804 same genomic locus (blue), the viral isolates OK35 & OK32 (yellow) or OK35 & OK26 (orange)
805 containing tags on separate genomic loci and the viral isolate OK31 containing two tag
806 sequences on a single viral genome (gray). **(A and B)** Each column represents the average
807 relative overlapping area calculated from all cells (with detectable overlap) infected under the
808 same condition. Error bars represent standard error of the means. *P < 0.05, ***P < 0.001; by
809 t test. **(C and D)** Individual cells were plotted to compare the relative overlapping area to the
810 nuclear area. All analyses were conducted on images generated from three independent
811 experimental repeats done on different days with viral stocks prepared and tittered separately.

812 **Figure 5. Nuclear size correlates with the number of RCs per cell.** Cells were co-infected
813 with the viral recombinants OK35 & OK25 (blue), OK35 & OK32 (yellow) and OK35 & OK26
814 (orange). Comparing the mean number of RCs per cell **(A)** and the mean nuclear area **(B)**
815 between Vero (bright coloured columns) and U2OS (dark coloured columns). Error bars
816 represent standard error of the means. **(C-H)** Individual Vero **(C, E, G)** and U2OS **(D, F, H)**
817 cells were plotted to compare the number of RCs per cells **(C, D)**, the total area of RCs per
818 cell **(E, F)** and the average area of each RCs **(G, H)** to the nuclear area. A trend line (colour
819 coded as above) was calculated using the ordinary least squares (OLS) method is presented
820 for each infection condition. All analyses were conducted on images generated from three

821 independent experimental repeats done on different days with viral stocks prepared and
822 tittered separately.

823 **Figure 6. Inhibition of RC movement reduces the rate of HR recombination.** Vero **(A)** or
824 U2OS **(B)** cells were co-infected with the viral recombinants OK35 & OK25 (blue), OK35 &
825 OK32 (yellow) and OK35 & OK26 (orange) in the presence (empty bar) or absence (full bar)
826 of Latruncalin B. Progeny viruses from each infection condition were plated for individual
827 plaques and colors were quantitated. The percent of dual color plaques out of the total
828 fluorescent plaques were measured. The averages are shown from two individual plaque
829 plating, from two technical repeats in two separate experiments. Error bars represent standard
830 error of the means. *P < 0.05, ***P < 0.001; by t test.

831 **Figure 7. Replication compartments contain at least one tag sequence.** Representative
832 images of U2OS cells infected with two viral isolates containing tag sequences at different
833 genomic loci (OK35 and OK32). The cells were hybridized with two probes conjugated to three
834 distinct fluorophores. I. Detection of the OK35 tag sequence is shown in red. II. Detection of
835 the OK32 tag sequence is shown in green. III. Detection of the viral 'a' sequence (detect HSV
836 DNA non-specifically) is shown in blue. Overlays of two and three colours are shown in panels
837 IV and V, respectively. DAPI is presented in gray. Scale bar is 5 μm.

838 ***Supplementary table 1. Accumulated data from image analysis program outputs.*** *Data*
839 *from 3 experiments for each cell type was collected. Each line represents individual cell. For*
840 *each cell, the following parameters are listed: the number of RCs in that cell, the number of*
841 *colocalization events, the area of the nucleus, the total area of all RC, the total area of*
842 *colocalization events, the adjusted RC area (total area of the RCs minus the area of*
843 *colocalization which removes measuring the area of colocalization in both colors) and the ratio*
844 *between area of colocalization to adjusted RC area.*

845

Viral recombinant	Tag sequence	Locus of insertion	Insertion start point
OK25	SV40p:YPET	Between the ORFs UL3 and UL4	11736
OK26	SV40p:YPET	Between the ORFs UL55 and UL56	116153
OK32	SV40p:YPET	Between the ORFs UL37 and UL38	84252
OK31	SV40p:YPET CMVp:mCherry	Between the ORFs UL55 and UL56 Between the ORFs UL37 and UL38	116153 84252
OK35	CMVp:mCherry	Between the ORFs UL37 and UL38	11736

846 **Table 1. List of viral recombinants used in this work**

847

848

SV40p:YPET	CMVp:mCherry	HSV-1 a' sequence
CTTGCATCTCAATTAGTCAGCAACC	CTTAAGCCCATATATGGAGTTCCGC	CCCCCCGCTCCTCCCCCCGCT
GCTACGGCGTGCAGTGCTTCGCCAG	TAACTTACGGTAAATGGCCCGCCTG	
TCCGCCCATTCTCCGCCCCATCGCT	AACGACCCCCGCCCATTGACGTCAA	
ATTTATGCAGAGGCCGAGGCCGCCT	GACGTATGTTCCCATAGTAACGCCA	
CCTCTGAGCTATTCCAGAAGTAGTGAGG	GACTTTCCATTGACGTCAATGGGTG	
GGAGGCCTAGGCTTTTGCAAAAAGC	CGGTAAACTGCCCACTTGGCAGTAC	
GACACAACAGTCTCGAATTTAAGGCTAG	ATGGGCGTGGATAGCGGTTTGACTC	
CTGTTCACCGGAGTGGTGCCTATCC	CCAAAATGTCGTAACAACTCCGCCC	
CGACGCTACCTACGGAAAGCTGACC	ATGGGCGGTAGGCGTGTACGGTGGG	
GTGCCTTGGCCCACCCTTGTGACCA	GCAGAGCTGGTTTAGTGAACCGTCA	
ACCACATGAAGCAGCACGACTTCTT	GATAACATGGCCATCATCAAGGAGT	
AACATCCTGGGCCACAAGCTGGAGT	GTGGATAGCGGTTTGACTCACGGG	
CATCACCGCCGACAAGCAGAAGAAC	GTCCCCTCAGTTCATGTACGGCTCC	
CCCATCGGCGACGGTCCCGTGCTGC	GTGGTGACCGTGACCCAGGACTCCT	
CCTGACAACCACTACCTGAGCTACCAG	GGACGGCGAGTTCATCTACAAGGTG	
TTCAAGGACCCCAACGAGAAGCGGG	CCCGTAATGCAGAAGAAGACCATGG	
CACGACTGTGCCTTCTAGTTGCCAG	CTCCGAGCGGATGTACCCCGAGGAC	
GACCCTGGAAGGTGCCACTCCCACT	CGGCGCCTACAACGTCAACATCAAG	
GGAAATTGCATCGCATTGTCTGAGT	GTCTCCACCCCATTGACGTCAATGG	
GGAAGACAATAGCAGGCATGCTGGG	CATCGCTATTACCATGGTGATGCGG	

849 **Table 2. List of fluorescently labelled probes for FISH.**

850

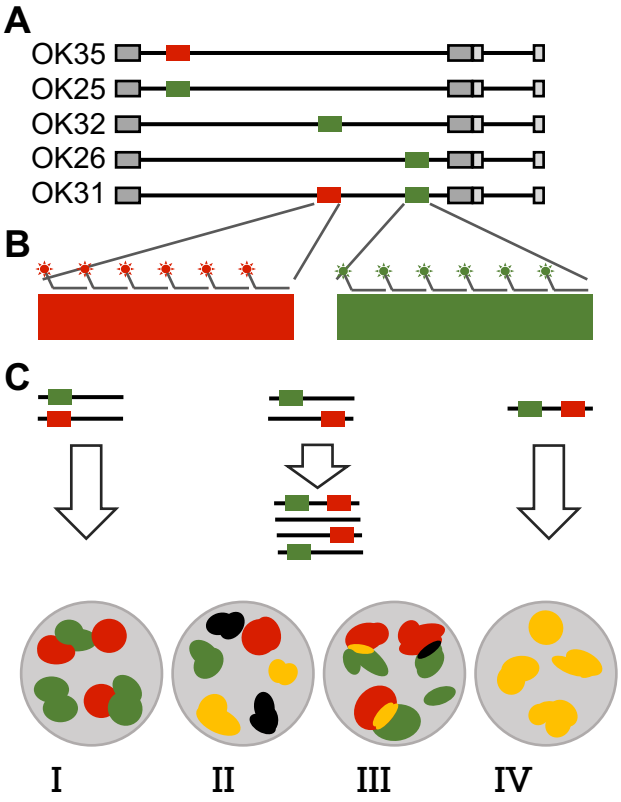
A
OK35
OK25
OK32
OK26
OK31
B
C
I
II
III
IV

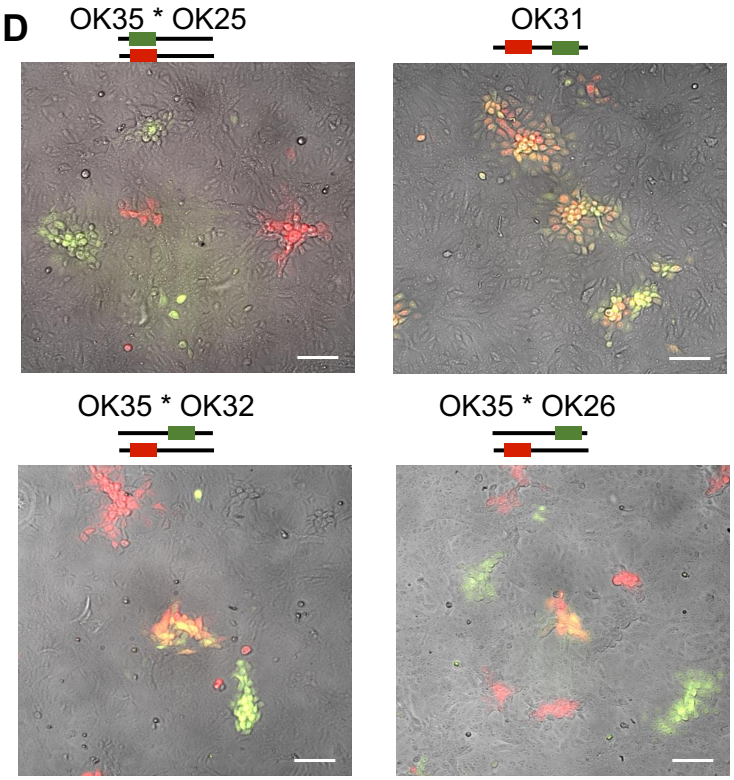
D
OK35 * OK25
OK31
OK35 * OK32
OK35 * OK26

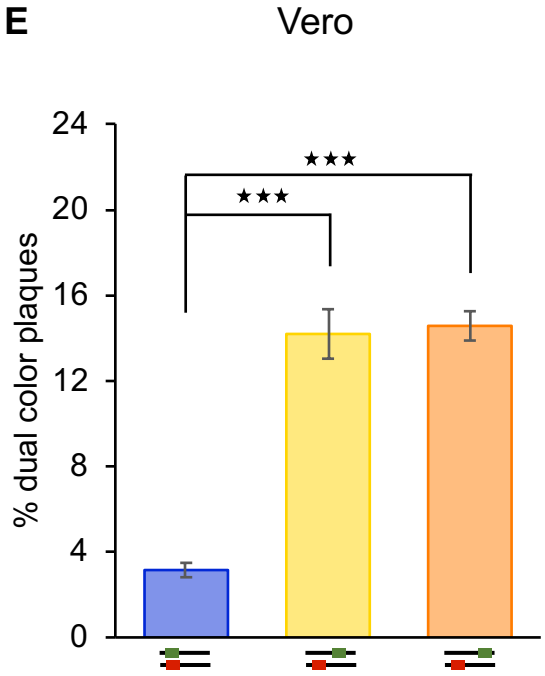
E
Vero
% dual color plaques
0
4
8
12
16
20
24
★★★
★★★

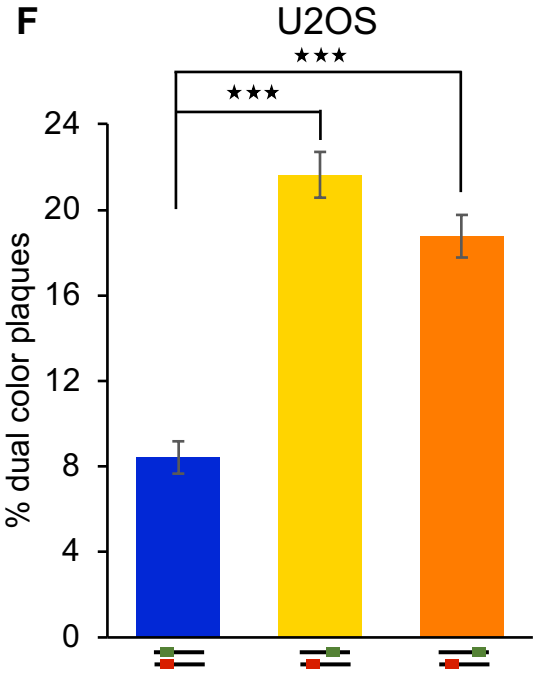
F
U2OS
% dual color plaques
0
4
8
12
16
20
24
★★★
★★★

Figure 1

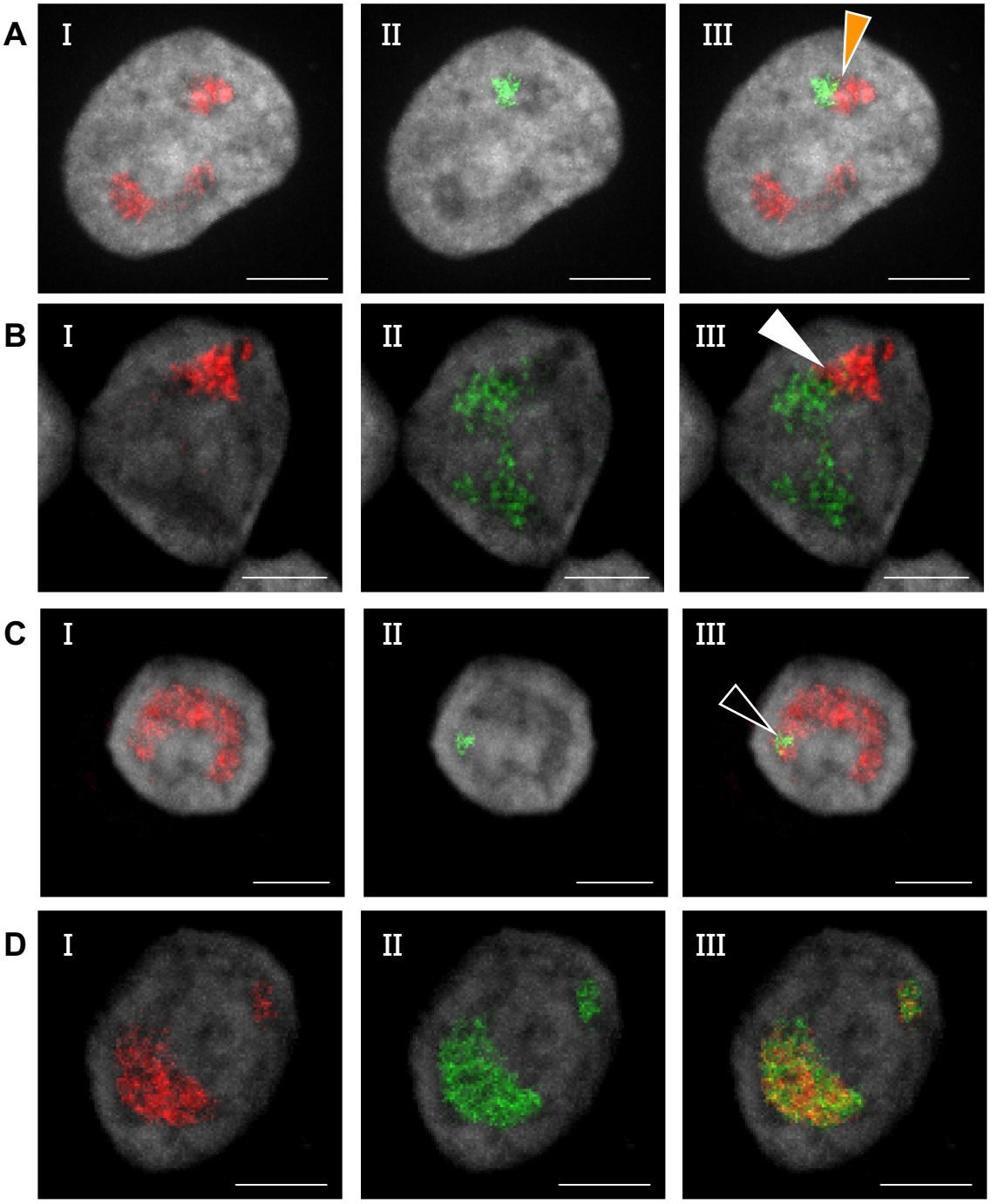

E

	A – minimal overlap	B - periphery overlap	C- Full overlap within larger RC	D – Full overlap
OK25*OK35	40.4 (±2.2)	50.9 (±0.4)	5.4 (±1.2)	3.3 (±1.4)
OK32*OK35	24.9 (±5.2)	66.9 (±5.0)	4.6 (±0.4)	3.5 (±0.5)
OK26*OK35	24.5 (±4.5)	67.2 (±2.1)	5.0 (±2.9)	3.3 (±0.9)
OK31	2.4 (±1.7)	3.7 (±0.5)	3.5 (±3.3)	90.4 (±4.4)

Figure 2

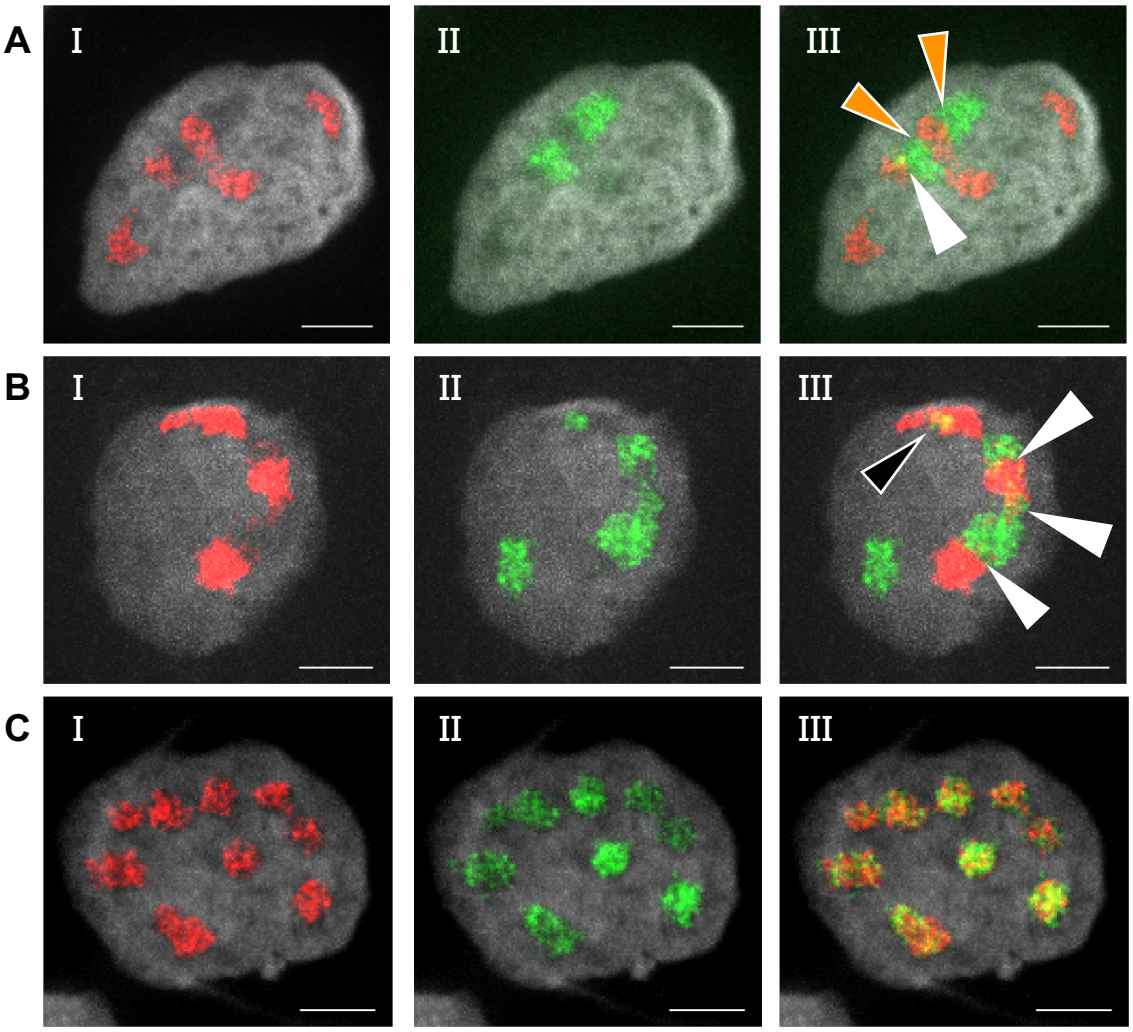

D

	A – minimal overlap	B - periphery overlap	C- Full overlap within larger RC	D – Full overlap
OK25*OK35	40.4 (±3.6)	55.2 (±1.5)	3.9 (±2.8)	0.5 (±0.8)
OK32*OK35	24.4 (±5.1)	72.0 (±5.0)	2.3 (±0.8)	1.4 (±0.7)
OK26*OK35	26.5 (±4.9)	71.4 (±4.6)	1.7 (±0.9)	0.5 (±0.4)
OK31	1.6 (±1.0)	3.7 (±0.7)	0.6 (±1.0)	94.1 (±2.2)

Figure 3

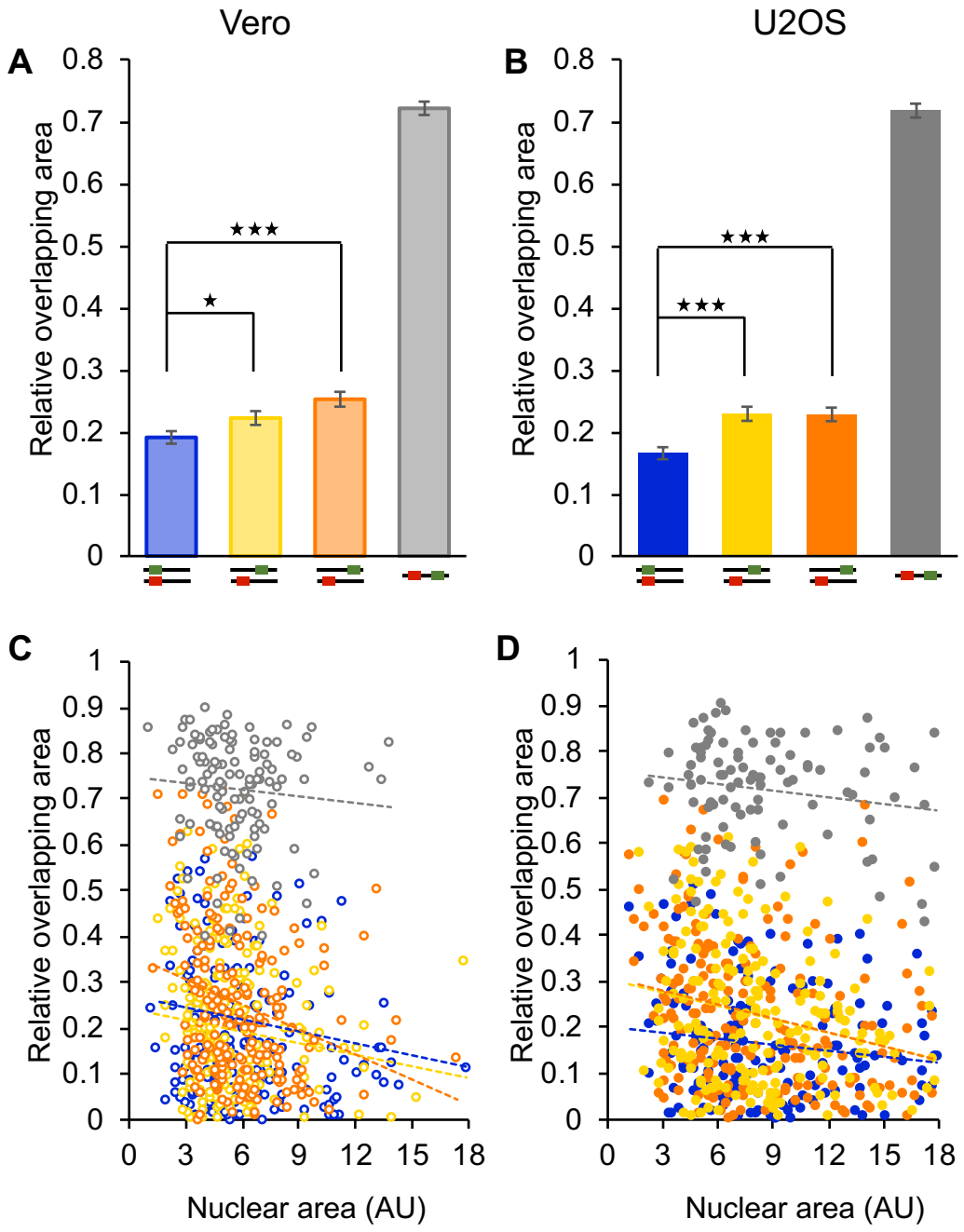
Vero
U2OS
A
B
C
D
Relative overlapping area
0.8
0.7
0.6
0.5
0.4
0.3
0.2
0.1
0
★★★
★
★★★
★★★
1
0.9
0
3
6
9
12
15
18
Nuclear area (AU)

Figure 4

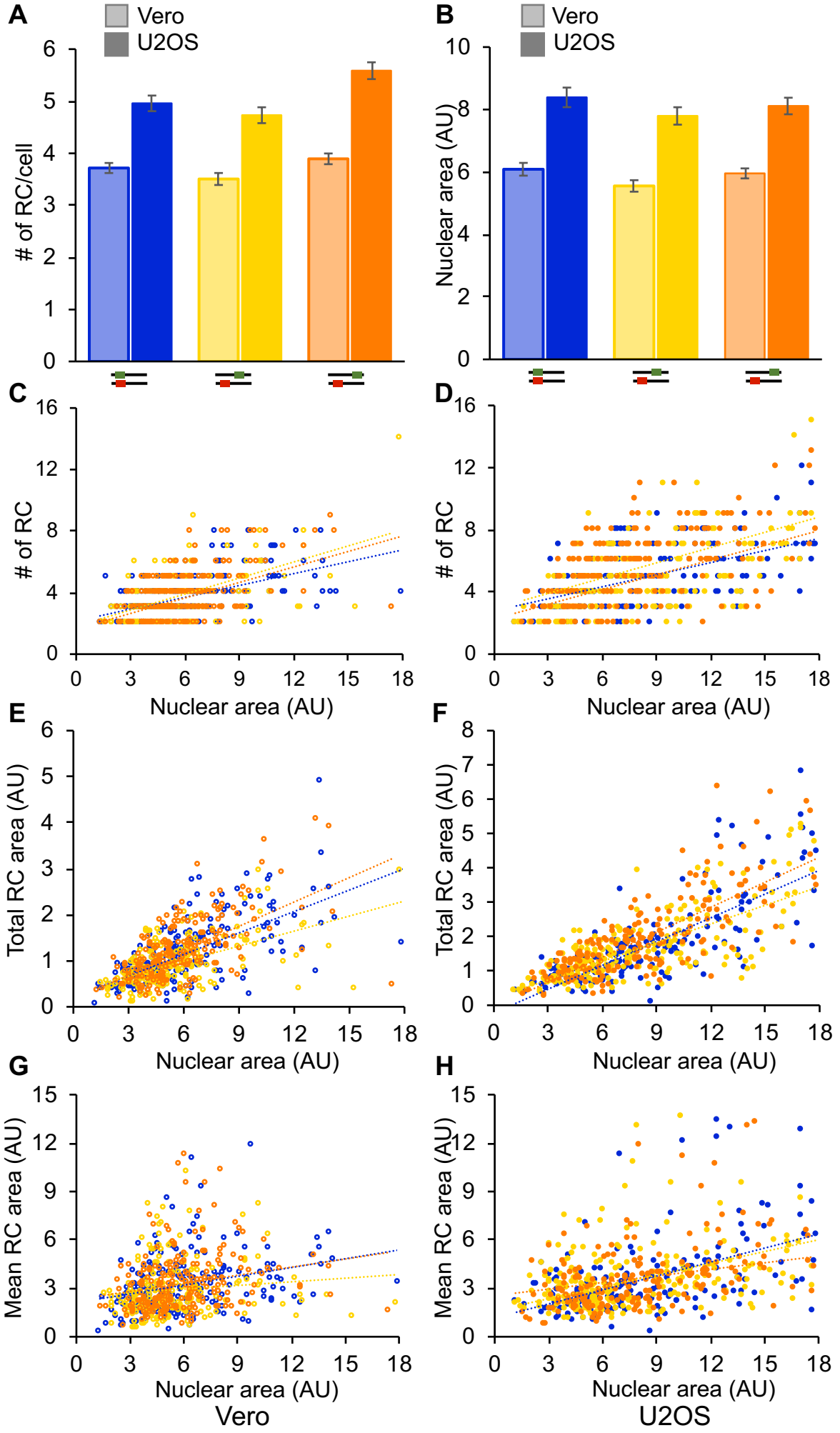
A
Vero
U2OS
# of RC/cell
B
Vero
U2OS
Nuclear area (AU)
C
# of RC
Nuclear area (AU)
D
# of RC
Nuclear area (AU)
E
Total RC area (AU)
Nuclear area (AU)
F
Total RC area (AU)
Nuclear area (AU)
G
Mean RC area (AU)
Nuclear area (AU)
Vero
H
Mean RC area (AU)
Nuclear area (AU)
U2OS

Figure 5

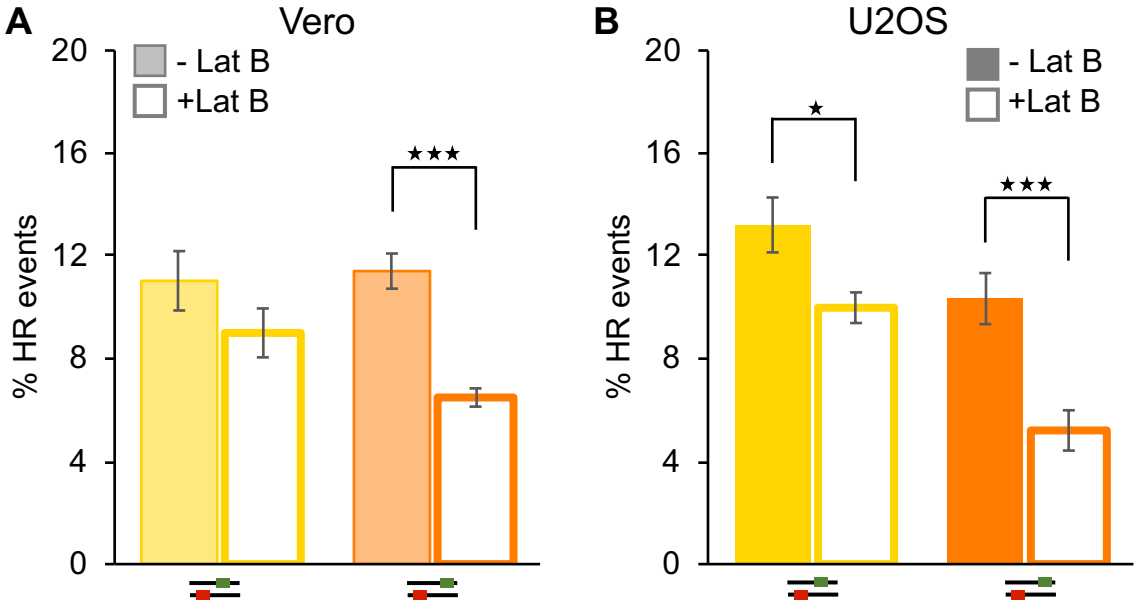
A
Vero
- Lat B
+Lat B
% HR events
20
16
12
8
4
0
★★★
B
U2OS
- Lat B
+Lat B
% HR events
20
16
12
8
4
0
★
★★★

Figure 6

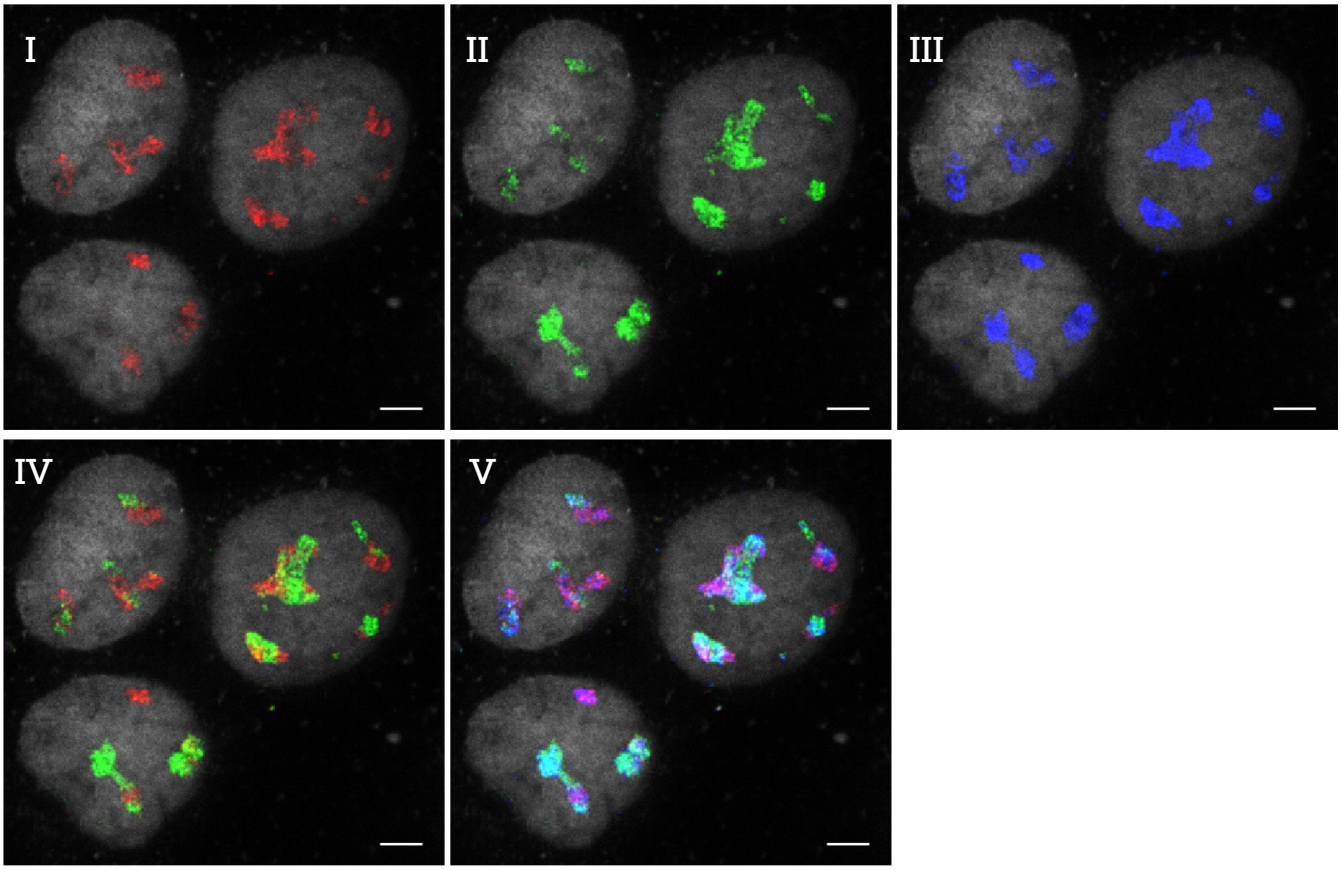

Figure 7